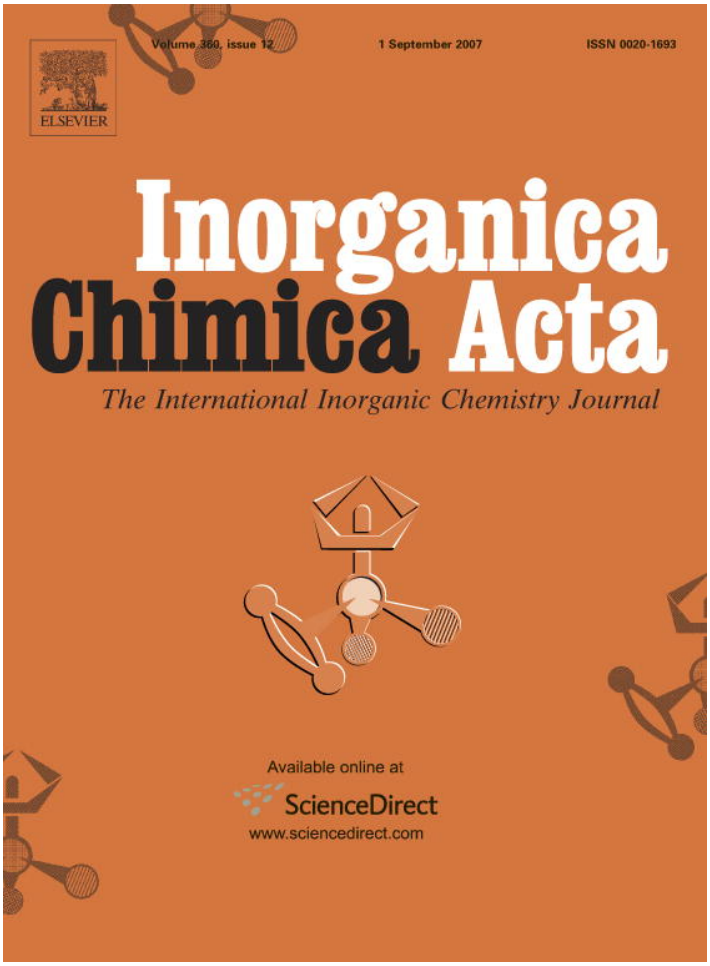

Available online at www.sciencedirect.com
ScienceDirect
Inorganica Chimica Acta 360 (2007) 3733–3740
Inorganica Chimica Acta
www.elsevier.com/locate/ica

Synthesis and characterization of tetrakis(μ-hydroxo)tetrakis(2,2′-dipicolylamine)tetranickel perchlorate, a nickel-hydroxy cubane complex

Jeffrey P. Wikstrom [a], Alexander Y. Nazarenko [b], William M. Reiff [c,*], Elena V. Rybak-Akimova [a,*]

[a] Department of Chemistry, Tufts University, Medford, MA 02155, United States
[b] Department of Chemistry, State University of New York, College at Buffalo, 1300 Elmwood Avenue, Buffalo, NY 14222, United States
[c] Department of Chemistry and Chemical Biology, Northeastern University, Boston, MA 02115, United States

Received 11 April 2007; received in revised form 8 May 2007; accepted 8 May 2007
Available online 16 May 2007

Abstract

A novel tetranuclear complex, $[Ni(\mu_3\text{-}OH)(DPA)]_4(ClO_4)_4$ (where DPA = 2,2′-dipicolylamine) has been synthesized, with characterization including electronic and infrared spectroscopy, elemental analysis, mass spectrometry, crystal structure analysis, and variable-temperature and variable-field magnetic susceptibility measurements. The complex features a 4Ni–4OH cubane-type cluster, displaying both ferromagnetic and antiferromagnetic intracluster interactions in a 2*J* model ($J_1 = -3.4\ cm^{-1}$, $J_2 = 4.7\ cm^{-1}$, $D = 2.0\ cm^{-1}$). Each nickel atom sits in a pseudooctahedral environment, with one DPA molecule facially coordinated and the remaining three coordination sites occupied by the bridging hydroxide anions that make up the cubane core.

Keywords: Nickel complexes; Aminopyridine ligands; Hydroxo-bridged cubane

1. Introduction

Polynuclear metal complexes have become a major area of study over the last 20 years, due largely to their variety of potential applications. Such clusters show possibilities as catalytic materials [1–3], as biomimetic systems for study of enzyme active sites or metal storage systems such as ferritin [4], and as magnetic materials [5–11]. Single-molecule magnets (SMMs) are currently the subject of intense interest. Their potential utility for study of quantum tunneling [6–8], for use in developing nanoscale information storage devices, quantum computers [6,9], and a host of related potential applications, has led to an explosion of recent developments in the area of polynuclear , magnetically coupled coordination clusters. One motif showing promise as an SMM or potential SMM is the nickel-hydroxy cubane-type tetranuclear cluster [12–14] first crystallographically identified in 1969 [15]. Recent interest has led to its library of examples increasing significantly in the past few years.

Many of these new nickel cubane clusters are supported by a polydentate ligand such as 2-pyridyl-methoxide [12,14,16–18], which features a nitrogen donor atom that in the cluster binds to one site of the octahedral nickel, and an alkoxy group that participates in the cluster by bridging among three nickel centers. With three sites participating in the cubane cluster and one site coordinated to the nitrogen of the ligand, two sites remain open for coordination by an anion, or by an alcohol molecule, the identity of which influences the cluster's magnetic properties [12,14].

This motif, in which the ligand system participates directly in the cubane-type cluster, appears popular

* Corresponding authors. Tel.: +1 617 627 3413; fax: +1 617 627 3443 (E.V. Rybak-Akimova).
E-mail address: elena.rybak-akimova@tufts.edu (E.V. Rybak-Akimova).

0020-1693/$ - see front matter © 2007 Elsevier B.V. All rights reserved.
doi:10.1016/j.ica.2007.05.013

[19–21] inasmuch as it directs the formation of a polynuclear metal system, rather than a nickel monomer. Its success suggests a somewhat different possible design strategy, one encouraging formation of polynuclear clusters supported by monodentate bridging ligands. The three binding sites of a tridentate ligand occupy half the coordination sphere of an octahedral metal center; chelation of a single tridentate ligand to an octahedral metal center leaves three sites open for coordination by monodentate ligands. A facially coordinating tridentate ligand permits formation of a cubane-type cluster with methoxy or hydroxy anions.

We present a nickel cubane-type cluster prepared following that strategy: no alkoxy bridges are incorporated in the polydentate ligands, and hydroxy bridges are exclusively responsible for the cluster formation. It is a 4Ni–4OH cubane-type cluster supported by a scaffolding of 2,2′-dipicolylamine, with four perchlorate counterions. The nickel-hydroxy cage moiety at the center of this complex has only three prior examples in the literature that have been magnetically characterized [22–25]. Along with the preparation, characterization, and magnetic properties of the new cubane, we compare our results to previously reported data.

2. Experimental

2.1. Materials

All materials were purchased from Sigma–Aldrich and used as received. Elemental analysis was performed by Desert Analytics, Inc. Infrared spectra of the solid were recorded, in KBr pellets, on a Mattson RS-1 FTIR spectrometer. UV–Vis spectra were acquired on a Hitachi U-2000 spectrophotometer or on a JASCO V-570 spectrophotometer. UV–Vis spectra of the solid were obtained by measurement of diffuse reflectance of pure solid sample. MS analysis was performed by electrospray mass spectrometry using a Finnigan LTQ (San Jose, CA) LCQ ion trap mass spectrometer in the positive ion detection mode.

2.2. $[(Ni(\mu_3\text{-}OH)DPA)_4](ClO_4)_4$ (1)

To a stirred, chilled (0 °C) ethanolic solution of 160 mg (4.0 mmol) NaOH and 0.199 g (0.18 mL, 1.0 mmol) DPA was added an ethanolic solution of 365 mg (1 mmol) nickel(II) perchlorate hexahydrate. The resulting blue precipitate was immediately filtered out of the mixture, dried, redissolved in acetonitrile (~5 mL), and filtered again to remove any traces of $Ni(OH)_2$. Large clear blue crystals of $\mathbf{1} \cdot 3(CH_3CN)$ were grown from this solution using ether diffusion at 4 °C over a period of three days. Yield: 600 mg (40%). Selected IR data (KBr pellet, cm^{-1}): 3443 (br), 2920 (s), 2366 (w), 2225 (m), 1592 (s), 1576 (m), 1484 (s), 1443 (s), 1385 (w), 1341 (w), 1311 (w), 1286 (w), 125 (w), 1096 (vs), 1027 (m), 978 (m), 913 (m), 765 (s), 641 (s), 625 (s), 505 (w), 483 (w), 418 (s). Electronic spectra in acetonitrile, λ_{max} (ε calculated per mole of **1**): 595 nm (sh), 659 nm (43), 770 (26), 972 (64). *m/z*: 1397. *Anal.* Calc. for $\mathbf{1} \cdot 2H_2O$ ($C_{48}H_{60}N_{12}O_{22}Cl_4Ni_4$): C, 37.59; H, 3.94; N, 10.96; Ni, 15.31. Found: C, 37.40; H, 4.21; N, 11.22; Ni, 15.93%.

2.3. Crystallographic data collection and structure refinement

A suitable crystal of $\mathbf{1} \cdot 3(CH_3CN)$ was mounted on a glass fiber using paratone oil. Data were collected using a Bruker SMART CCD (charge-coupled device) based diffractometer equipped with an LT-3 low-temperature apparatus operating at 173 K. Data were measured using omega scans of 0.3° per frame for 30 s, such that a hemisphere was collected. A total of 1650 frames were collected with a maximum resolution of 0.75 Å and processed using SAINT [26] (correcting for Lorentz and polarization effects) and SADABS [27] (applying absorption corrections) software. The structure was solved by direct methods using SHELXS-97 [28] and refined by least-squares using SHELXL-97 [29]. All non-hydrogen atoms were refined anisotropically. One of the acetonitrile molecules occupies two positions in agreement with the position of the neighboring disordered perchlorate ion. Positions of hydrogen atoms were calculated and refined as a riding model. A summary of the data collection and refinement is given in Table 1.

2.4. Magnetic susceptibility studies

Direct current (dc) magnetic susceptibility measurements were made on polycrystalline powder samples using a Quantum Design (MPMSXL) SQUID magnetometer at

Table 1
Crystallographic data for compound $\mathbf{1} \cdot 3(CH_3CN)$

Formula	$C_{54}H_{65}Cl_4N_{15}Ni_4O_{20}$
Formula weight	1620.77
Space group	*Pbca*
Unit cell dimensions	
a (Å)	24.326(5)
b (Å)	21.764(6)
c (Å)	26.243(5)
α (°)	90
β (°)	90
γ (°)	90
V (Å^3)	13894(5)
Z	8
λ (Mo Kα)	0.71073
Crystal size (mm)	$0.20 \times 0.15 \times 0.10$
T (K)	173(2)
h,*k*,*l* Range collected	$0 \geqslant h \geqslant 28$, $0 \geqslant k \geqslant 25$, $0 \geqslant l \geqslant 31$
μ	1.301
Number of unique reflections	12218
Reflections ($F > 2.0\sigma$)	4739
Number of parameters	947
Number of restraints	782
wR_2	0.1966
R_1	0.0709
Goodness-of-fit	0.827
Largest diffraction	0.876/−0.729

Northeastern University. Magnetic susceptibilities were corrected for the background signal of the sample holder and for diamagnetic susceptibilities of all atoms. The dc susceptibility data was recorded in three experiments, between 2 and 300 K (95 data points) at 10 000 Oe, between 2 and 36 K (67 data points) at 10 000 Oe, and, in a variable-field experiment, between 2 and 8 K at 2500, 5000, and 10 000 Oe.

3. Results and discussion

Synthesis of **1** (as shown in Fig. 1) was done by combining an ethanolic solution of nickel(II) perchlorate hexahydrate with 1 equiv. of 2,2′-dipicolylamine (DPA) and 4 equiv. of NaOH (an excess over the stoichiometrically required 1 equiv.). The resulting light blue complex **1** precipitated out of the ethanol solvent immediately, and was crystallized from acetonitrile solution.

The compound was characterized by CHN and Ni elemental analysis, by UV/Vis and IR spectroscopy in the solid state and by UV/Vis in acetonitrile solution. Crystals grown by ether diffusion were analyzed with X-ray diffraction. Magnetic susceptibility studies were also performed on solid (powder) samples.

3.1. Description of the crystal structure of $\mathbf{1}\cdot 3(CH_3CN)$

The asymmetric unit is made up of the cationic $[Ni_4(\mu_3\text{-}OH)_4(DPA)_4]^{4+}$, four ClO_4^- counterions, and three molecules of solvent CH_3CN. The $[Ni_4(\mu_3\text{-}OH)_4(DPA)_4]^{4+}$ metal cluster unit (see Fig. 2) includes a cubane-type 4Ni–4OH cluster constructed from four nickel atoms and four hydroxide groups on alternating corners. Each nickel atom is crystallographically distinct, in a distorted octahedral environment which varies slightly for each metal center. Each nickel atom is coordinated to three nitrogen atoms, two pyridine and one amine, all part of the tridentate DPA ligand, as well as three of the hydroxide groups which make up the cubane core. The bond distances and angles are summarized in Table 2. The Ni–N(am) distances range from 2.09 to 2.11 Å while Ni–N(py) bonds are 2.08–2.11 Å. Each of the three hydroxides in the coordination sphere of each nickel atom yields a Ni–O bonding distance ranging from 2.04 to 2.08 Å with an average value of 2.064 in perfect agreement with the average of Ni–O bond lengths (2.065 A) in 54 Ni_4O_4 clusters found in the Cambridge Structure database [30]. O–Ni–O angles are systematically lower than 90°, again in agreement with the 81.7 ± 2 in reported structures (see Supplementary material). Correspondingly, Ni–O–Ni angles are significantly higher, with two of them in a range of 97–99° and the third being around 101°. This is again in satisfactory agreement with known data (mean 98° with standard deviation of 3°). Geometric constraints imposed by the cubane core reduce

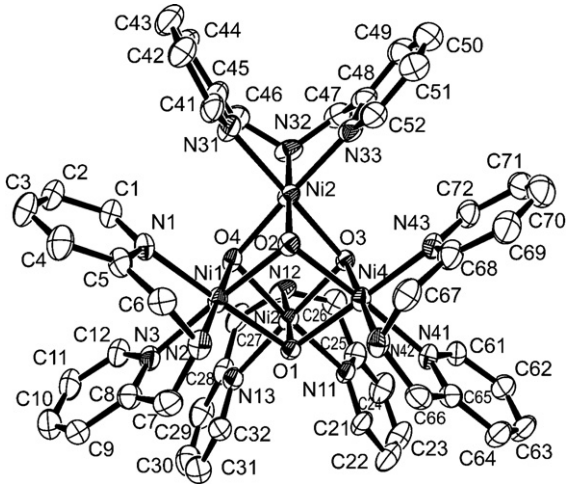

Fig. 2. ORTEP diagram of $\mathbf{1}\cdot 3CH_3CN$, with hydrogens, solvent, and counterions omitted for clarity. Metric parameters (CIF file) available in Supplementary material.

Table 2
Selected bond lengths (Å) and angles (°) for **1**

Ni1–O4	2.035(5)	O4–Ni1–O2	81.50(19)
Ni1–O2	2.081(5)	O4–Ni1–O1	81.89(17)
Ni1–O1	2.084(4)	O2–Ni1–O1	78.21(18)
Ni1–N1	2.084(6)	O1–Ni2–O4	81.89(18)
Ni1–N2	2.104(6)	O1–Ni2–O3	80.07(18)
Ni1–N3	2.105(7)	O4–Ni2–O3	78.66(18)
Ni2–O1	2.049(5)	O2–Ni3–O4	81.35(19)
Ni2–O4	2.070(4)	O2–Ni3–O3	81.21(18)
Ni2–O3	2.072(5)	O4–Ni3–O3	78.50(18)
Ni2–N13	2.086(7)	O3–Ni4–O1	80.67(18)
Ni2–N11	2.111(6)	O3–Ni4–O2	81.36(18)
Ni2–N12	2.113(6)	O1–Ni4–O2	79.11(18)
Ni3–O2	2.051(5)	Ni4–O1–Ni1	101.5(2)
Ni3–O4	2.072(5)	Ni2–O1–Ni1	96.29(18)
Ni3–O3	2.078(4)	Ni3–O2–Ni4	97.46(19)
Ni3–N33	2.079(7)	Ni3–O2–Ni1	97.2(2)
Ni3–N32	2.091(6)	Ni4–O2–Ni1	100.7(2)
Ni3–N31	2.100(6)	Ni4–O3–Ni2	98.35(19)
Ni4–O3	2.047(5)	Ni4–O3–Ni3	97.57(19)
Ni4–O1	2.049(5)	Ni2–O3–Ni3	101.05(19)
Ni4–N43	2.076(6)	Ni1–O4–Ni2	97.14(19)
Ni4–O2	2.076(4)	Ni1–O4–Ni3	98.0(2)
Ni4–N41	2.081(6)	Ni2–O4–Ni3	101.29(19)
Ni4–N42	2.106(6)		

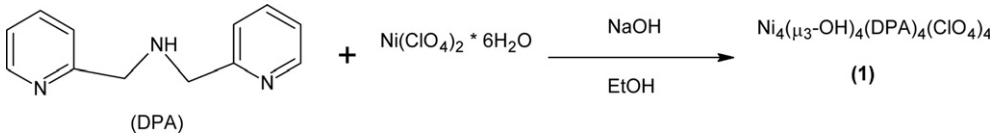

Fig. 1. Synthesis of **1**.

Ni–O–Ni angles from the ideal tetrahedral value of 109.5°, a reduction often associated with ferromagnetic coupling of nickel centers.

The three-dimensional structure of $\mathbf{1} \cdot 3CH_3CN$ reveals a network of weak non-covalent interactions. Each hydrogen atom present in the hydroxy anions of the central cluster is connected via a weak hydrogen bond to the corresponding perchlorate ion; hydrogen atoms of amino groups are connected via hydrogen bonds to the nitrogen atoms of two acetonitrile molecules. The remaining perchlorate is disordered; the acetonitrile molecule that occupies the residual void in a crystal cell is forced to occupy two different locations to fit each of the possible positions of perchlorate ion.

3.2. Spectroscopic results

Direct infusion MS of a micromolar solution of **1** shows a peak family around 1397 m/z matching the isotopic distribution expected for $[Ni_4(\mu_3\text{-}OH)_4(DPA_4)(ClO_4)_3]^+$: 1393 (29), 1394 (17), 1395 (78), 1396 (46), 1397 (100), 1398 (60), 1399 (84), 1400 (46), 1401 (48), 1402 (24), 1403 (22), 1404 (12), 1405 (8), 1407 (6), 1409 (6), thus confirming that the cluster remains intact in solution.

The electronic spectra of **1** in acetonitrile show the following peaks (ε): 595 nm (sh), 659 nm (29), 770 (16), 972 (40). These bands are consistent with trigonally-distorted octahedral nickel: $D_q = 1029\ cm^{-1}$, $B = 1061\ cm^{-1}$, $\beta = 0.97$, parameters calculated using the technique described by Gahan [31]. The peak at 972 nm is assigned to the $^3A_{2g} \rightarrow {}^3T_{2g}$ transition (generally expected in the region 1020–800 nm for nickel(II)) and the peak at 659 nm is assigned to the $^3A_{2g} \rightarrow {}^3T_{1g}(F)$ transition. The smaller peak at 770 nm may be assigned to the spin-forbidden $^3A_{2g} \rightarrow {}^1E_g$ transition. The resulting parameters are very consistent with those expected for octahedral nickel(II) exhibiting interactions with multiple nitrogen donors [32]. A solid-state UV/Vis spectrum shows the same system of peaks, indicating the structure about the nickels is the same in solution and solid state.

A solution of $[Ni(DPA)_2](ClO_4)_2$ in acetonitrile, the only previously characterized nickel(II) DPA complex [33–35], shows bands at 515 nm and 800 nm, regions absent absorbance bands in the spectrum of **1**. This indicates that **1**, both in solution and in the solid state, contains no nickel(II) in the 1:2 metal:DPA species, and is entirely consistent with the crystallographic data.

3.3. Magnetic results

Dc susceptibility data was recorded in two experiments, with T ranging from 2 to 300 K and 2 to 36 K. The resulting data show good reproducibility. As shown in Fig. 3, the data show a maximum χ_M of $0.34\ cm^3\ mol^{-1}$ at 7.8 K, decreasing below that temperature and dropping to $0.015\ cm^3\ mol^{-1}$ at room temperature (300 K), a $\chi_M * T$ of $4.5\ cm^3\ K\ mol^{-1}$. Four isolated Ni^{2+} centers are predicted to have a spin-only $\chi_M * T$ of $4.4\ cm^3\ K\ mol^{-1}$ ($g = 2.2$). The decrease in χ_M as temperature decreases from 7.8 K suggests significant contribution from the zero-field splitting parameter D in that temperature range. While the magnetic moment μ is approximately 3.0 Bohr magnetons at room temperature, as would be predicted for four non-interacting nickel(II) atoms, this value declines to 1.0 BM at 1.8 K.

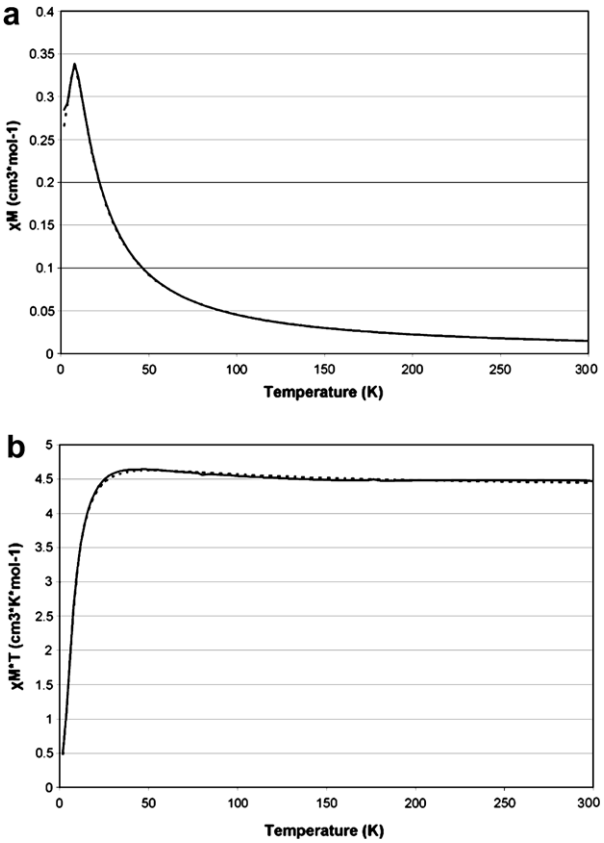

Fig. 3. Plot of (a) χ_M against T and (b) $\chi_M * T$ against T for a powder sample of (**1**), where χ_M is the molar magnetic susceptibility. The solid lines mark the experimental data; the dashed lines mark a fit of the Van Vleck equation to the data for the solution set $J_1 = -3.4\ cm^{-1}$; $J_2 = 4.7\ cm^{-1}$; $D = -2.0\ cm^{-1}$; $g = 2.08$.

The data can be fit simultaneously using Kambe's vector-coupling method for magnetic exchange [36] as modified by Vicente et al. [37] to account for the D contribution, within an $S = 4$ four-metal system modeling the four nickel clusters as a pair of dimers. No acceptable fit could be obtained for a single J, while a set of two J parameters matched the experimental data. The magnetic exchange was treated with two J-parameters, as shown in Fig. 4

$$H = -2J_1(S_1S_2 + S_3S_4) - 2J_2(S_1S_3 + S_1S_4 + S_2S_3 + S_2S_4)$$

Application of the Van Vleck equation to the appropriate Hamiltonian leads to the equation

$$\chi_M = \frac{Ng^2\beta^2}{3kT} * \frac{\sum S_i(S_i+1)(2S_i+1)\exp(-E_i/kT)}{\sum(2S_i+1)\exp(-E_i/kT)}$$

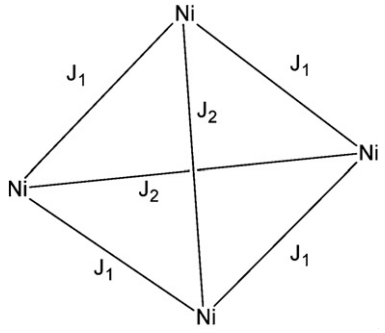

Fig. 4. Scheme illustrating the two-J model of a tetranickel system, after [37].

where the values for S and E for each of the 19 energy levels are those derived and tabulated by Vicente and co-workers [37] following the method of Kambe [36]. A full examination of this method and its general applicability for magnetic interactions in discrete polynuclear paramagnetic clusters can be found in the review by Sinn [38]. The zero-field splitting term is substituted for the ground-state term ($E_i = 0$), an approximation incorporating zero-field splitting into the susceptibility equation at the ground state only; zero-field splitting is approximated to contribute only for $E_i = 0$. Modeling the data with three unique J-parameter variables (following the method of Gray and co-workers [39]) did not substantively improve the fit.

The two sets of data were fit simultaneously to the equation and values for J_1, J_2, D, and g extracted. Two different solution sets are approximately equally good fits by the least-squares method. The first $J_1 = -3.4\ \mathrm{cm}^{-1}$; $J_2 = 4.7\ \mathrm{cm}^{-1}$; $D = -2.0\ \mathrm{cm}^{-1}$; $g = 2.08$ indicates antiferromagnetic coupling between the nearest nickel neighbors and ferromagnetic coupling with the more distant metal centers. The second solution set $J_1 = 5.4\ \mathrm{cm}^{-1}$; $J_2 = -0.1\ \mathrm{cm}^{-1}$; $D = -2.2\ \mathrm{cm}^{-1}$, and $g = 2.09$ shows ferromagnetic coupling between the nearest neighbors and essentially zero antiferromagnetic interaction with the more distant neighbors. Both solution sets indicate strong contribution from the D zero-field-splitting parameter.

The data above 20 K was also fit to the 2J model derived from Kambe without the zero-field splitting modification introduced by Vicente et al., with g fixed at 2.09. The least-squares fit of the data yielded the parameters $J_1 = -4.2\ \mathrm{cm}^{-1}$; $J_2 = 3.8\ \mathrm{cm}^{-1}$. This indicates antiferromagnetic coupling between the nearest nickel neighbors and ferromagnetic coupling with the more distant metal centers, consistent with the first solution set described above. An inferior fit yields a second solution set $J_1 = 5.1\ \mathrm{cm}^{-1}$; $J_2 = -1.1\ \mathrm{cm}^{-1}$, which shows ferromagnetic coupling between the nearest neighbors and antiferromagnetic interaction with the more distant neighbors, corresponding to the second solution set described above but with a stronger antiferromagnetic interaction to correct for the lack of a zero-field splitting term. The superior fitting of the first solution set implies that an antiferromagnetic J_1 and ferromagnetic J_2 are more accurate than a ferromagnetic J_1 and antiferromagnetic J_2; this would seem to indicate the solution set $J_1 = -3.4\ \mathrm{cm}^{-1}$; $J_2 = 4.7\ \mathrm{cm}^{-1}$; $D = -2.0\ \mathrm{cm}^{-1}$; $g = 2.08$ found above is preferable to its alternative.

Dc susceptibility from 2 to 8 K was measured at 2500 Oe, 5000 Oe, and 10 000 Oe, and this low-temperature data fit to the equation resulting from the application of the Van Vleck equation to the Hamiltonian for zero-field splitting in an $S = 4$ environment [37,40]:

$$H = D[S_z^2 - S(S+1)/3]$$

Fitting the low-temperature variable-field data to the resulting equation with g fixed at 2.09 results in a D parameter of $-0.77\ \mathrm{cm}^{-1}$, the same sign and approximate magnitude as the D values generated from the fixed-field experiment.

This is in keeping with established trends for nickel cubane-type clusters (see Supplementary material). Ferromagnetic coupling tends to be the norm, as would be expected for ~90° Ni–O–Ni bond angles; this is consistent with familiar trends. Antiferromagnetic coupling is most often seen correlating to Ni–O–Ni bond angles approaching 100° [41–43]. Christou et al. have examined magneto-structural correlations for 4Ni–4OR cubane complexes [44], which forms the basis of this examination. Two-J fits recognizing two Ni–Ni interactions and therefore two discrete faces of the cubane core, an axial and an equatorial, are most common, indicating that the majority of known nickel cubane clusters display two distinct magnetic interactions [12,17,20,21,24,43–51]. These can result in either two different ferromagnetic interactions [12,17,20,21,45,49,50], or in one ferromagnetic interaction and one antiferromagnetic interaction [20,21,24,44,46–48,50]; these two cases are both reported with equal frequency, while there are no examples of a wholly antiferromagnetic two-J fit. All nickel cubane species share a distorted cubic prism moiety; this overall cubic shape imposes geometric constraints that result in a narrow distribution of bond angles in the series of compounds. Internal geometry thus varies only within an approximately 10° range (from ~89 to ~101°). These relatively small structural variations are reflected in the relatively narrow range of extant J-values reported, which are all within $40\ \mathrm{cm}^{-1}$ (from -20 to $+20\ \mathrm{cm}^{-1}$). However, this variance of structure is not the only factor to which J parameters can be assigned; cubanes with very similar geometry may have different J-values when coordinated to different ligand systems [33].

3.4. 4Ni–4OH cubane clusters

While numerous examples of 4Ni–4OMe and 4Ni–4OR cubane-type clusters have been presented [12,14–19,22–25,39,41–48,50–70] (see Supplementary material), only a handful of magnetically characterized 4Ni–4OH clusters can be found in the literature, particularly excepting

polyoxometallates, which may include a nickel cubane subunit as a part of a larger polyoxometallic core. These are summarized in Table 3.

The magnetic properties of the first extant 4Ni–4OH cubane cluster, $[Ni(OH)(chta)]_4^{4+}$ (chta = cyclohexane-1,3,5-triamine) (Fig. 6) were described by Boyd et al. [22], though the complex's synthesis and structure were originally characterized by Aurivillius [23]. The complex possesses relatively high symmetry, with each nickel in the cubane coordinated to one tridentate cyclohexane-1,3,5-triamine ligand that occupies all three open sites of the metal in a facial arrangement. The magnetic data was modeled using a 3J system: $J_1 = -0.80\ cm^{-1}$, $J_2 = -1.16\ cm^{-1}$, $J_3 = 0.95\ cm^{-1}$.

The second example of a hydroxy cubane, $(Ni_4(OH)_4(tzdt)_4(py)_4) \cdot 2py$ (tzdt = 1,3-thiazolidine-2-thionate, py = pyridine) (Fig. 7) features a dihedral ligand system, in which the bidentate 1,3-thiazolidine-2-thionate ligand is coordinated to two different nickels, across the diagonal of the cubane face [24]. Each metal center is in this way supported by two different molecules of thionate, at two of the three open coordination sites, the other three being occupied by bridging hydroxy groups. A molecule of solvent pyridine occupies the remaining site. The magnetic model used describes two sets of coupling: a ferromagnetic J_1 ($17.5\ cm^{-1}$) accounting for two of the three nickel–nickel interactions experienced by each metal center in the cluster, and an antiferromagnetic J_2 ($-22\ cm^{-1}$) accounting for the remaining interaction, perhaps paralleling the two ligand-bridged nickel pairs each metal center participates in; $g = 2.0$.

Much like the prior example, the third hydroxy cubane, $[Ni_4(pypentO)(pym)(\mu_3\text{-}OH)_2(\mu\text{-}OAc)_2(NCS)_2(OH_2)]$ (pypentO = 1,5-bis[(2-pyridylmethyl)amino]pentane-3-oxide, pym = 2-pyridylmethoxide) (Fig. 8), is supported by multiple species of bridging ligand [25]: in addition to the four hydroxyl groups coordinating within the cubane core, two acetate anions coordinate in a bridging fashion each to two nickel centers, on opposite faces of the cubane. A molecule of 2-pyridyl methoxide coordinates to one metal center and donates an alkoxy group to the cubane, while a molecule of 1,5-bis[(2-pyridylmethyl)amino]pentane-3-ol deprotonated at the oxygen coordinates to two nickels on the opposite side of the cubane. Thiocyanate coordinates to the remaining nickel's two open sites. The result is a low-symmetry complex comprising a nickel–oxygen cubane-type cluster wherein two of the four cubane oxygens are hydroxy oxygens, and two are alkoxy oxygens provided by the coordinating ligands. The magnetic data was fit using three J parameters: $J_1 = -3.1\ cm^{-1}$, $J_2 = 15\ cm^{-1}$, $J_3 = 6.7\ cm^{-1}$, $g = 2.27$. This correlates to exchange across the two acetate-bridged faces of the

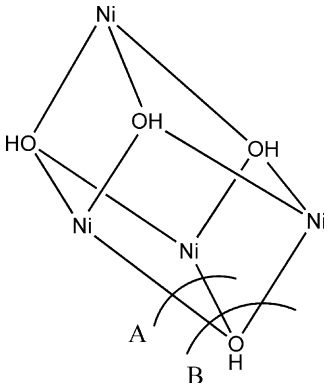

Fig. 5. Diagram showing relationship of selected angles *A* and *B* in Table 2.

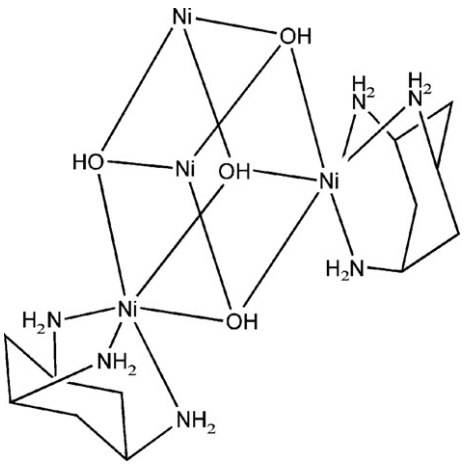

Fig. 6. Illustration of schematic structure of $[Ni(OH)(chta)]_4^{4+}$ [22]. Two chta groups are omitted for clarity (chta = cyclohexane-1,3,5-triamine).

Table 3
Known 4Ni–4OH cubane-type clusters

Ligand(s) 4Ni–4OH	Coordinated	Present	*J*			*g*	*D*	Selected Ni–O–Ni angles (see Fig. 5)		Reference
								Angle A	Angle B	
A		NO_3	−0.57	−0.8	−1.16	2.2		98.3	99.7	[22,23]
B	pyridine		17.5	−22		2.0		95.6	103	[24]
C	thiocyanate, acetate		−2.98	14.97	10.9	2.23	0.011	89.4	99.8	[25]
D		perchlorate	−3.4	4.7		2.08	−2	96.1	100	this work

A: 1,3,5-Triaminocyclohexane.
B: 1,3-Thiazolidine-2-thionate.
C: 1,5-Bis[(2-pyridylmethyl)amino]pentane-3-oxide.
D: 2,2′-Dipicolylamine.

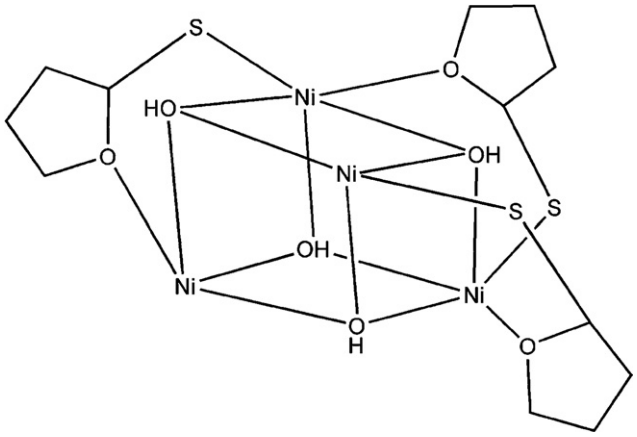

Fig. 7. Illustration of binding scheme of $(Ni_4(OH)_4(tzdt)_4(py)_4) \cdot 2py$ [24]. The pyridine groups and one tzdt group are omitted for clarity (tzdt = 1,3-thiazolidine-2-thionate, py = pyridine).

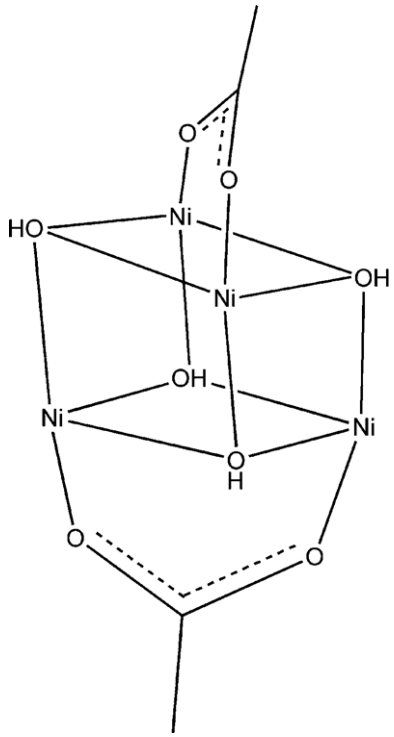

Fig. 8. Illustration of binding scheme of bridging acetate groups of the nickel cubane core of $[Ni_4(pypentO)(pym)(\mu_3\text{-}OH)_2(\mu\text{-}OAc)_2(NCS)_2(OH_2)]$ [25] (pypentO = 1,5-bis[(2-pyridylmethyl)amino]pentane-3-oxide, pym = 2-pyridylmethoxide).

cubane being ferromagnetic, and the exchange across the faces without acetate bridges being antiferromagnetic. This is consistent with the prior example, and the presence of a bridging group exterior to the cubane cluster causing antiferromagnetic interaction. It should be noted that this species is not a 4Ni–4OH cubane but a 4Ni–2OH–2HOR material; it incorporates two alkoxy groups into the central core.

The novel nickel cubane (**1**) possesses this same unusual 4Ni–4OH motif, and lacks a bridging component exterior to the cubane in the manner of two of the three prior examples. In an architecture similar to the remaining example, each metal center's six coordination sites are divided into two categories; three are occupied by the bridging hydroxy groups which make up the core of the cubane, and three are coordinated to a single tridentate ligand which chelates facially. Unlike many of the polydentate ligands so common among 4Ni–4OR cubane-type clusters, DPA is neutral, and so the cluster comprised of four Ni^{2+} and four OH^- units has four associated perchlorate counterions. Magnetic studies of the material indicate a sizable zero-field splitting contribution to susceptibility at low temperatures, and both ferromagnetic and antiferromagnetic exchange with $J_1 = -3.4\ cm^{-1}$; $J_2 = 4.7\ cm^{-1}$; $D = -2.0\ cm^{-1}$; $g = 2.08$ (though other solution sets are possible from least-squares fitting). These J-values are within the range of reported coupling parameters for 4Ni–4OH cubane-type clusters (see Table S1 in Supplementary material) though weaker than the coupling reported for clusters featuring anionic tridentate ligands and stronger than the previously reported example of a 4Ni–4OH cubane-type cluster featuring a neutral tridentate ligand.

4. Summary

We here described a 4Ni–4OH cubane-type cluster formed from a familiar tridentate ligand 2,2′-dipicolylamine (DPA), and thus added to the small field of nickel-hydroxide cubane chemistry. DPA and $[Ni(DPA)_2]^{2+}$ [33–35] are well-known compounds, but this new material assembles in the presence of an additional bridging ligand:hydroxide. Its magnetic behavior is consistent with that of other known nickel cubanes, with weak intracluster ferromagnetic and antiferromagnetic exchange. Further investigations making use of this synthetic pathway are underway.

Appendix A. Supplementary material

Supplementary data associated with this article can be found, in the online version, at doi:10.1016/j.ica.2007.05.013.

References

[1] P. Sobota, Coord. Chem. Rev. 248 (2004) 1047.
[2] M.G. White, Catalysis 18 (2005) 72.
[3] J. Taquet, O. Siri, P. Braunstein, R. Welter, J. Am. Chem. Soc. 45 (2006) 4668.
[4] A.K. Powell, Compr. Coord. Chem. II 8 (2004) 169.
[5] D. Gatteschi, R. Sessoli, A. Cornia, Chem. Commun. 9 (2000) 725.
[6] K.M. Mertes, Y. Suzuki, M.P. Sarachik, Y. Myasoedov, H. Shtrikman, E. Zeldov, E.M. Rumberger, D.N. Hendrickson, G. Christou, Recent Res. Dev. Phys. 4 (2003) 731.
[7] K.M. Mertes, Y. Suzuki, M.P. Sarachik, Y. Myasoedov, H. Shtrikman, E. Zeldov, E.M. Rumberger, D.N. Hendrickson, G. Christou, Solid State Commun. 127 (2003) 131.
[8] M.A. Novak, J. Magn. Magn. Mater. 272–276 (2004) E707.

[9] M. Cavallini, J. Gomez-Segura, D. Ruiz-Molina, M. Massi, C. Albonetti, C. Rovira, J. Veciana, F. Biscarini, Angew. Chem., Int. Ed. 44 (2005) 888.
[10] D. Gatteschi, A.L. Barra, A. Caneschi, A. Cornia, R. Sessoli, L. Sorace, Coord. Chem. Rev. 2505 (2006) 1514.
[11] N.E. Chakov, S. Lee, A.G. Harter, P.L. Kuhns, A.P. Reyes, S.O. Hill, N.S. Dalal, W. Wernsdorfer, K.A. Abboud, G. Christou, J. Am. Chem. Soc. 128 (2006) 6975.
[12] E.C. Yang, W. Wernsdorfer, S. Hill, R.S. Edwards, M. Nakano, S. Maccagnano, L.N. Zakharov, A.L. Rheingold, G. Christou, Polyhedron 22 (2003) 1727.
[13] M. Nakano, G. Matsubayashi, T. Muramatsu, T.C. Kobayashi, K. Amaya, J. Yoo, G. Christou, D.N. Hendrickson, Mol. Cryst. Liquid Cryst. 376 (2002) 405.
[14] E.C. Yang, W. Wernsdorfer, L.N. Zakharov, Y. Karaki, A. Yamaguchi, R.M. Isidro, G.D. Lu, S.A. Wilson, A.L. Rheingold, H. Ishimoto, D.N. Hendrickson, Inorg. Chem. 45 (2006) 529.
[15] J.E. Andrew, A.B. Blake, J. Chem. Soc. A 10 (1969) 1456.
[16] E. del Barco, A.D. Kent, E.C. Yang, D.N. Hendrickson, Polyhedron 24 (2005) 2695.
[17] D.N. Hendrickson, E.C. Yang, R.M. Isidro, C. Kirman, J. Lawrence, R.S. Edwards, S. Hill, A. Yamaguci, H. Ishimoto, W. Wernsdorfer, C. Ramsey, N. Dalal, M.M. Olmstead, Polyhedron 24 (2005) 2280.
[18] C. Kirman, J. Lawrence, S. Hill, E.C. Yang, D.N. Hendrickson, J. Appl. Phys. 97 (2005) 10M501/1.
[19] A.K. Sah, C.P. Rao, P.K. Sarrenketo, K. Rissanen, Chem. Lett. 12 (2001) 1296.
[20] A. Sieber, C. Boskovic, R. Bircher, O. Waldmann, S.T. Oschsenbein, G. Chaboussant, H.U. Guedel, N. Kirchner, J. van Slageren, W. Wernsdorfer, A. Neels, H. Stoeckli-Evans, S. Janssen, Inorg. Chem. 44 (2005) 4315.
[21] C. Boskovic, E. Rusanov, H. Stoeckli-Evans, H.U. Gudel, Inorg. Chem. Commun. 5 (2002) 881.
[22] P.D.W. Boyd, R.L. Martin, G. Schwarzenback, Aust. J. Chem. 41 (1988) 1449.
[23] B. Aurivillius, Acta Chem. Scand. 31 (1977) 501.
[24] L. Ballester, E. Coronado, A. Gutierrez, A. Monge, M.F. Perpinan, E. Pinilla, T. Rico, Inorg. Chem. 31 (1992) 2053.
[25] J.M. Clemente-Juan, B. Chansou, B. Donnadieu, J.P. Tuchagues, Inorg. Chem. 39 (2000) 5515.
[26] G.M. Sheldrick, Bruker Analytical X-ray System, Madison, WI 2001.
[27] G.M. Sheldrick, 1996.
[28] G.M. Sheldrick, Acta Crystallogr. A A46 (1990) 467.
[29] G.M. Sheldrick, 1997.
[30] F.H. Allen, Acta Crystallogr. B58 (2002) 380.
[31] T.M. Donlevy, L.R. Gahan, R. Stranger, S.E. Kennedy, K.A. Byriel, C.H.L. Kennard, Inorg. Chem. 32 (1993) 6023.
[32] H.J.G. Hernandez, T. Pandiyan, S. Bernes, Inorg. Chim. Acta 359 (2006) 1.
[33] M. Velusamy, M. Palaniandavar, K.R.J. Thomas, Polyhedron 17 (1998) 2179.
[34] S.M. Nelson, J. Rodgers, J. Chem. Soc. A 2 (1968) 272.
[35] A. Hazell, C.J. McKenzie, L.P. Nielsen, Polyhedron 19 (2000) 1333.
[36] K. Kambe, J. Phys. Soc. Jpn. 5 (1950) 48.
[37] A. Escuer, M. Font-Bardia, S.B. Kumar, X. Solans, R. Vicente, Polyhedron 18 (1999) 909.
[38] E. Sinn, Coord. Chem. Rev. 5 (1970) 313.
[39] W.L. Gladfelter, M.W. Lynch, W.P. Schaefer, D.N. Hendrickson, H.B. Gray, Inorg. Chem. 20 (1981) 2390.
[40] O. Kahn, Molecular Magnetism, Wiley-VCH, Inc., 1993.
[41] J.A. Bertrand, A.P. Ginsberg, R.I. Kaplan, C.E. Kirkwood, R.L. Martin, R.C. Sherwood, Inorg. Chem. 10 (1971) 240.
[42] G.S. Papaefstathiou, A. Escuer, F.A. Mautner, C. Raptopoulou, A. Terzis, S.P. Perlepes, R. Vicente, Eur. J. Inorg. Chem. 5 (2005) 879.
[43] T.A. Hudson, K.J. Berry, B. Moubaraki, K.S. Murray, R. Robson, Inorg. Chem. 45 (2006) 3549.
[44] M.A. Halcrow, J.S. Sun, J.C. Huffman, G. Christou, Inorg. Chem. 34 (1995) 4167.
[45] G. Chaboussant, R. Basler, H.U. Guedel, S. Ochsenbein, A. Parkin, S. Parsons, G. Rajaraman, A. Sieber, A.A. Smith, G.A. Timco, R.E.P. Winpenny, Dalton Trans. 17 (2004) 2758.
[46] G. Rajaraman, K.E. Christensen, F.K. Larsen, G.A. Timco, R.E.P. Winpenny, Chem. Commun. 24 (2005) 3053.
[47] W. Vreugdenhil, J.G. Haasnoot, J. Reedijk, Inorg. Chim. Acta 129 (1987) 205.
[48] G. Aromi, A.S. Batsanov, P. Christian, M. Helliwell, O. Roubeau, G.A. Timco, R.E.P. Winpenny, Dalton Trans. 23 (2003) 4466.
[49] E.C. Yang, C. Kirman, J. Lawrence, L.N. Zakharov, A.L. Rheingold, S. Hill, D.N. Hendrickson, Inorg. Chem. 44 (2005) 3827.
[50] M. Moragues-Canovas, M. Helliwell, L. Ricard, E. Riviere, W. Wernsdorfer, E. Brechin, T. Mallah, Eur. J. Inorg. Chem. 11 (2004) 2219.
[51] M.L. Tong, S.L. Zheng, J.X. Shi, Y.X. Tong, H.K. Lee, X.M. Chen, J. Chem. Soc., Dalton Trans. 8 (2002) 1727.
[52] K. Bizilj, S.G. Hardin, F. Bernard, P.J. Oliver, E.R.T. Tiekink, G. Winter, Aust. J. Chem. 39 (1986) 1035.
[53] B.Y. Kuyavskaya, I.N. Ivleva, M.A. Yampol'skaya, N.V. Gerbeleu, M.K. Veksel'man, Teor. Eksp. Khim. 22 (1986) 285.
[54] B.Y. Kuyavskaya, I.N. Ivleva, M.A. Yampol'skaya, N.V. Gerbeleu, M.K. Veksel'man, Teor. Eksp. Khim. 25 (1989) 339.
[55] J.A. Barnes, W.E. Hatfield, Inorg. Chem. 10 (1971) 2355.
[56] J.A. Bertrand, C. Marabella, D.G. VanDerveer, Inorg. Chim. Acta 26 (1978) 113.
[57] M. Sorai, M. Yoshikawa, N. Arai, H. Suga, S. Seki, J. Phys. Chem. Solids 39 (1978) 413.
[58] M.S. El Fallah, E. Rentschler, A. Caneschi, D. Gatteschi, Inorg. Chim. Acta 247 (1996) 231.
[59] A.J. Blake, E.K. Brechin, A. Codron, R.O. Gould, C.M. Grant, S. Parsons, J.M. Rawson, R.E.P. Winpenny, Chem. Commun. 19 (1995) 1983.
[60] M. Darenbourg, R.M. Buonomo, J.H. Reibenspies, Z. Kristallogr. 210 (1995) 469.
[61] V.A. Ovchynnikov, V.M. Amirkhanov, A.A. Kapshuk, T.Y. Silva, T. Glowiak, H. Kozlowski, Z. Naturforsch. B 53B (1998) 836.
[62] U. Mukhopadhyay, D. Ray, Indian J. Chem. 37A (1998) 191.
[63] S. Mukherjee, T. Weyhermuller, E. Bothe, K. Wieghardt, P. Chaudhuri, Eur. J. Inorg. Chem. 5 (2003) 863.
[64] T.K. Paine, E. Renschler, T. Weyermueller, P. Chaudhuri, Eur. J. Inorg. Chem. 5 (2003) 863.
[65] F. Papp, E. Bouwman, W.L. Driessen, R.A.G. de Graaff, J. Reedijk, J. Chem. Soc., Dalton Trans. (1985) 737.
[66] A.J. Atkins, A.J. Blake, M. Schroeder, Chem. Commun. 21 (1993) 1662.
[67] A.J. Atkins, D. Black, A.J. Blake, A. Marin-Becerra, S. Parsons, L. Ruiz-Ramirez, M. Schroeder, Chem. Commun. 4 (1996) 457.
[68] N. Hoshino, T. Ito, M. Nihei, H. Oshio, Chem. Lett. 8 (2002) 844.
[69] M. Nihei, N. Hoshino, T. Ito, H. Oshio, Polyhedron 22 (2003) 2359.
[70] H. Liu, H. Wang, D. Niu, Z. Lu, Synth. React. Inorg. Met. Org. Nano-Met. Chem. 35 (2005) 779.